Electronic Supplementary Information for:

A nearly perfect icosahedral Ir@Au_{12} superatom with superior photoluminescence obtained by ligand engineering

Katsuya Mutoh,*[a] Teppei Yahagi,[a] Shinjiro Takano,[b] Sonomi Kawakita,[a] Takeshi Iwasa,[c] Tetsuya Taketsugu,[c] Tatsuya Tsukuda*[b] and Takuya Nakashima*[a]

[a]Department of Chemistry, Graduate School of Science, Osaka Metropolitan University, Sumiyoshi-ku, Osaka 558-8585, Japan.

[b]Department of Chemistry, Graduate School of Science, The University of Tokyo, Bunkyo-ku, Tokyo 113-0033, Japan.

[c]Department of Chemistry, Faculty of Science, Hokkaido University, North 10 West 5, Sapporo, Hokkaido 060-0810, Japan.

Experimental Procedures

General. Electrospray ionization mass (ESI-MS) spectrometry was conducted with a JEOL AccuTOF LC-plus 4G. ^{1}H (300 MHz) and ^{31}P{^{1}H} (121 MHz) NMR spectra were recorded on a Bruker Avance300 nanobay. The chemical shifts in the ^{1}H NMR spectra were referenced to the residual proton signal of the solvent (CD_3CN: δ 1.94). The chemical shifts in the ^{31}P{^{1}H} NMR spectra were referenced to the signal of 85 % H_3PO_4 (δ 0.00) as an external standard. Absorption and photoluminescence spectra were measured using a JASCO V-670 and FP-8650 spectrophotometer, respectively, with a 1 cm quartz cuvette. Photoluminescent lifetime measurement was carried out with DeltaFlex (HORIBA) with a 367-nm LED (SpectraLED-370) as an excitation light source.

Differential pulse voltammetry (DPV) measurements were performed in a conventional three-electrode cell. A glassy carbon electrode (0.6 cm in diameter) was employed as a working electrode after polishing with 0.05 μm alumina on an alumina polishing pad attached to a glass plate. The electrode was rinsed with pure acetone and dried in air before use. A platinum wire was used as a counter electrode, and an Ag/Ag^+ reference electrode (Ag wire, 0.01 M $AgNO_3$, 0.10 M tetrabutylammonium hexafluorophosphate ($TBAPF_6$) in acetonitrile) was employed. Prior to each experiment, the solutions were deoxygenated by bubbling with Ar, and the Ar atmosphere was maintained throughout the course of the experiments. Optical grade solvents were used for all measurements. All potentials are referenced to the reversible formal potential for the ferrocene/ferrocenium (Fc/Fc^+) couple. ECstat302 potentiostat/galvanostat (EC Frontier, Inc.) under computer control (ECstat Basic software) was used for the DPV measurement. Samples were dissolved in the 0.1 M $TBAPF_6$ CH_2Cl_2 solution at a concentration of ~0.50 mM. Differential pulse voltammograms were recorded at room temperature and the following conditions: Potential increments: 4 mV; pulse amplitude: 50 mV; pulse width: 50 ms; sampling width: 50 ms; pulse period: 200 ms.

Chemicals and solvents were purchased from Fujifilm Wako Pure Chemical Industries, Sigma-Aldrich Japan, and Tokyo Chemical Industry Co., Ltd. All commercially available reagents were used as received.

Synthesis of $[IrAu_{12}(bbpe)_6]Cl_3$. Six 100 mL test tubes equipped with s magnetic stir bar were each charged with $(AuCl)_2$(bbpe) (15.0 mg × 6; 105 μmol in total). CH_2Cl_2 (15 mL × 6) was added to each test tube, and the solutions were stirred for 1 h at 0 ºC. Then, $[Ir(COD)Cl]_2$ (1.5 mg × 6; 13 μmol in total) was added to each test tube, and the solutions turned yellow. To each of the solutions was added a freshly prepared EtOH solution of $BH_3 \cdot C_4H_{11}N$ (3.8 mg in 0.5 mL × 6; 264 μmol in total) all at once. The color of the solutions gradually turned brown. After stirring for 65 h at 0 ºC, the solutions were collected in a recovery flask and evaporated to dryness. The brown residue was washed with hexane and then extracted with CH_2Cl_2. After filtration to remove insoluble compounds, the filtrate was evaporated to dryness. The residue was dissolved in a minimum amount of MeOH (~20 mL). The solution was purified by reverse phase column chromatography (Wakosil® 100C18) using a mixture of MeOH/TFA/DEA = (100/0.1/0.1

v/v%) as an eluent. The solvent was removed by evaporation, and the residue was washed with water. The collected fraction was further separated by HPLC using a mixture of MeOH/TFA/DEA = (100/0.1/0.1 v/v%) as an eluent. The solvent of the fractions was removed by evaporation, and the residue was washed with water. $[IrAu_{12}(bbpe)_6]Cl_3$ was obtained as an orange solid (7.9 mg, 1.6 μmol, yield: 9.1% based on Au, 5.9% based on Ir).

Synthesis of $[IrAu_{12}(bbpe)_6](PF_6)_3$. $[IrAu_{12}(bbpe)_6]Cl_3$ (6.2 mg, 1.3 μmol) was dissolved in 3 mL of EtOH. To the solution was added EtOH solution of $NaPF_6$ (6.2 mg, 37 μmol, 0.3 mL). After stirring 2h at room temperature, the precipitate was collected by centrifugation and washed with EtOH to give $[IrAu_{12}(bbpe)_6](PF_6)_3$ as an orange solid. The yield was 4.7 mg (70.2%). The obtained solid was recrystallized by the diffusion method with CH_2Cl_2/MeOH/Et_2O.

HPLC analysis. HPLC analysis was conducted with LaChrom Elite system (Hitachi, pump; L-2130, detector; L2455). A preparative reverse phase column (InertSustain C30, GL Science) was employed and an isocratic elution condition was carried out using optimized mobile phases composed of methanol containing TFA (0.1v/v%) and DEA (0.1v/v%). The flow rate was set to 5 mL/min. For a conventional separation.

DFT calculations. All calculations were carried out using Gaussian 16 suite of programs version C.02.[S1] DFT calculations were performed for the models of $[IrAu_{12}(bbpe)_6]^{3+}$ and $[IrAu_{12}(dppm)_6]^{3+}$ using B3LYP functional. Relativistic effective core potential LANL2DZ was used for Au and Ir atoms and the basis sets of other atoms were 6-31G*. Normal mode analysis was conducted using the analytical second derivatives of the optimized ground-state structures to confirm that each stationary point is a minimum. The NBO analysis was carried out using NBO7.0 program.[S2]

X-ray crystallography. Single-crystal X-ray diffraction experiment of the **$IrAu_{12}$-b** was performed using a Bruker D8 VENTURE diffractometer equipped with a IμS 3.0 microfocus sealed tube (Mo Kα) and a PHOTON 3 detector. Selected specimen was scooped on a MiTeGen micro loop with Paratone-N oil and was quickly frozen by cold-N_2 stream. The obtained diffraction data were corrected for Lorentz polarization and numerical absorption correction was done using APEX5 software. The initial phase was solved by using SHELXT and the structure was refined by SHELXL-2019.[S3] All non-hydrogen atoms were refined anisotropically and hydrogen atoms were treated as riding models. It was found that one PF_6 anion and solvent molecules were heavily disordered. These diffused electron densities were treated by SQUEEZE program on PLATON platform.[S4,S5] All aromatic rings were treated as rigid constraints (AFIX 66) and disordered ethyl linker moiety was treated by dividing the moiety into two conformations. CHECKCIF program does not generate neither A- nor B-level alerts. The final cif file was deposited on Cambridge Crystallographic Data Center (CCDC) with the deposition No. of 2415728.

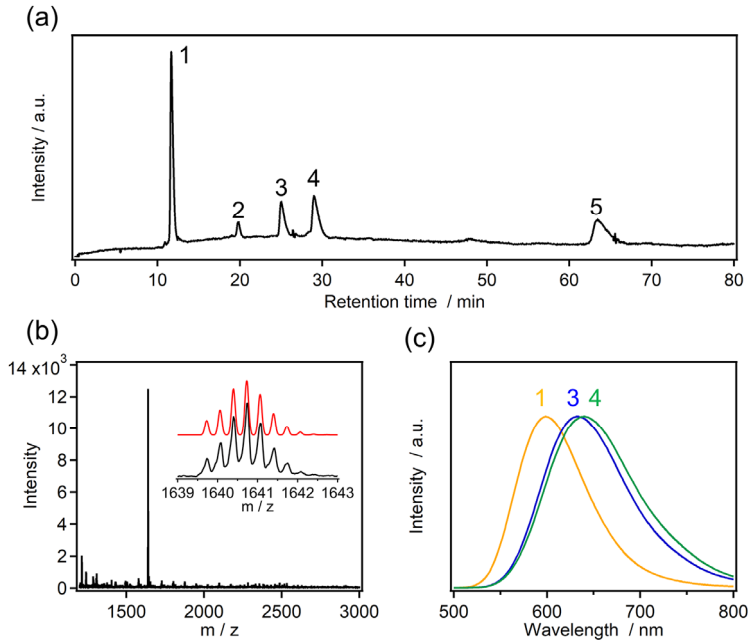

Fig. S1 (a) HPLC chromatogram for the as-synthesized mixtures for gold NCs. (b) HR-ESI-TOF-MS spectrum for the HPLC peak 1. The inset compares the experimental (black) and theoretical isotope patterns (red) for **IrAu$_{12}$-b**. (c) PL spectra of the HPLC fractions in CH_2Cl_2.

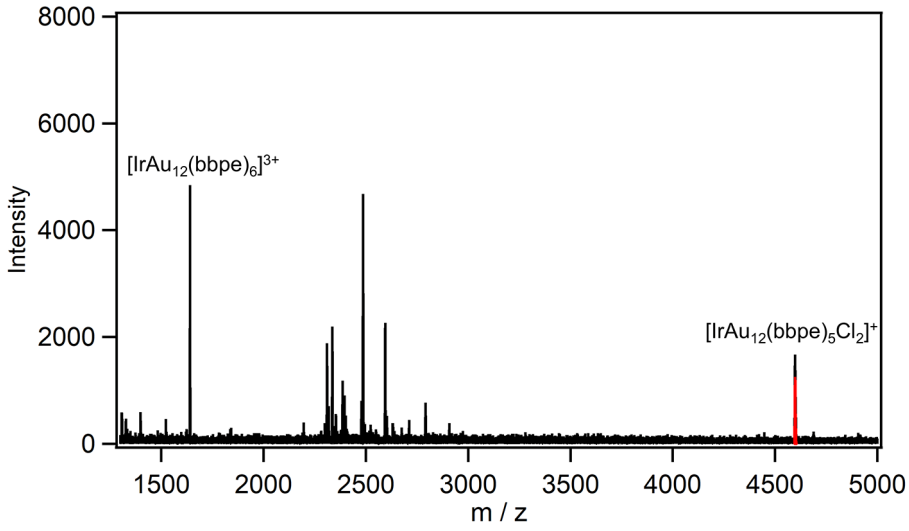

Fig. S2 ESI-TOF-MS spectrum for the fraction of the HPLC peak 4 in Fig. S2a. The red bar shows the simulation for $[IrAu_{12}(bbpe)_5Cl_2]^+$.

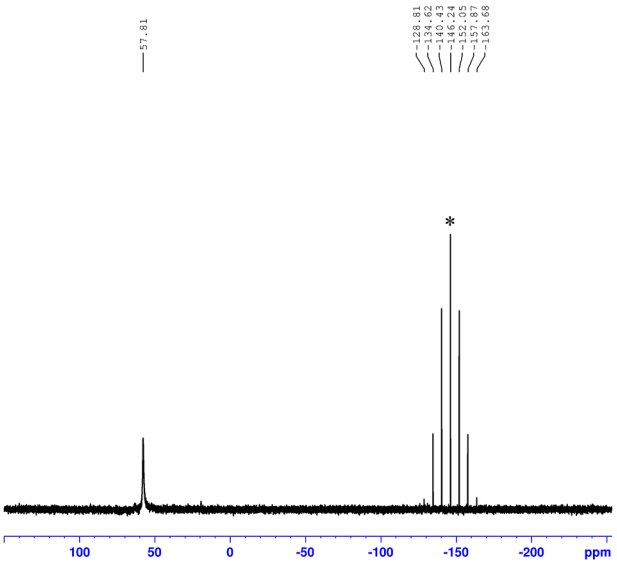

Fig. S3 $^{31}P\{^{1}H\}$ NMR spectrum of **IrAu$_{12}$-b** in CD_3CN (* PF_6).

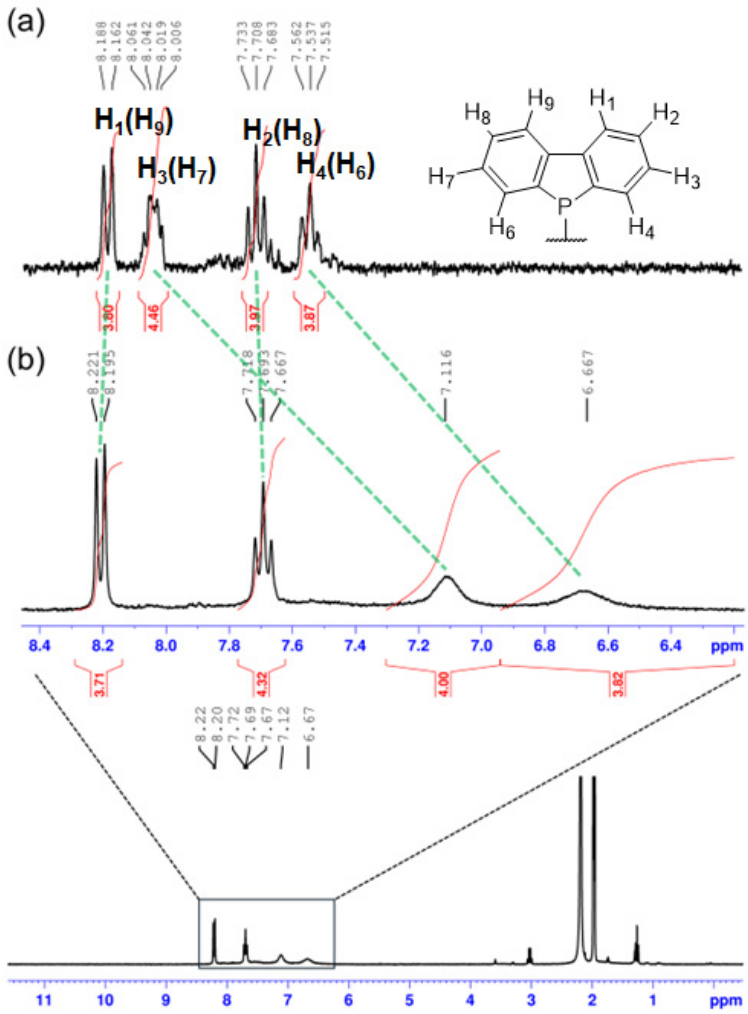

Fig. S4 ^{1}H NMR spectra of (a) $Au_2(bbpe)Cl_2$ in DMSO-d_6 and (b) **IrAu$_{12}$-b** in CD_3CN.

Table S1 CSM Values for M@Au_{12} Superatoms in the Reported Gold-based Clusters

cluster	CSM	ligand type	reference
$[IrAu_{12}(bbpe)_6]^{3+}$ (**$IrAu_{12}$-b**)	0.014	phosphine	this study
$[IrAu_{12}(dppm)_6]^{3+}$ (**$IrAu_{12}$-m**)	0.091	phosphine	S6
$[Au_{13}(dppm)_6]^{5+}$	0.568	phosphine	S7
$[RuAu_{12}(dppm)_6]^{2+}$	0.061	phosphine	S6
$[RhAu_{12}(dppm)_6]^{3+}$	0.079	phosphine	S6
$[Au_{13}(dppe)_5Cl_2]^{3+}$	0.036	phosphine	S8
$[RhAu_{12}(dppe)_5Cl_2]^{+}$	0.016	phosphine	S9
$[PdAu_{12}(dppe)_5Cl_2]^{2+}$	0.020	phosphine	S9
$[IrAu_{12}(dppe)_5Cl_2]^{+}$	0.030	phosphine	S10
$[IrAu_{12}(dppe)_5Br_2]^{+}$	0.020	phosphine	S11
$[IrAu_{12}(dppe)_5I_2]^{+}$	0.026	phosphine	S11
$[PtAu_{12}(dppe)_5Cl_2]^{2+}$	0.025	phosphine	S9
$[Au_{13}(dppe)_5(PA)_2]^{3+}$	0.021	phosphine	S12
$[IrAu_{12}(dppe)_5(PA)_2]^{+}$	0.018	phosphine	S13
$[PdAu_{12}(dppe)_5(PA)_2]^{2+}$	0.013	phosphine	S13
$[Au_{13}(dppe)_5(EPTpy)_2]^{3+}$	0.019	phosphine	S14
$[Au_{13}(R/S\text{-}dipamp)_5Cl_2]^{3+}$	0.049	phosphine	S15
$[Au_{13}(S\text{-}dipamp)_4(S\text{-}dipamp)Cl_2]^{3+}$	0.028	phosphine	S15
$[IrAu_{12}(R/S\text{-}dipamp)_5Cl_2]^{+}$	0.020	phosphine	S16
$[Au_{13}(PNP)_5Cl_2]^{3+}$	0.186	phosphine	S17
$[Au_{13}Cu_1(TBBT)_6(DPPF)_3]^{+}$	0.083	phosphine	S18
$[Au_{13}(PNP)_4(CN)_4]^{+}$	0.044	phosphine	S19
$[Au_{13}(AsPh_3)_8Cl_4]^{+}$	0.056	arsine	S20
$[Au_{13}(dpap)_5Cl_2]^{3+}$	0.045	arsine	S21
$[Au_{13}(SbPh_3)_8Cl_4]^{+}$	0.029	stibine	S22
$[Au_{13}(Bzim^{Bn})_9Cl_3]^{2+}$	0.031	NHC	S23
$[Au_{13}(R\text{-}Bzim\text{^}MeBz\text{^}Pi)_8Br_4]^{+}$	0.066	NHC	S24
$[Au_{13}(Bzim^{Bn})_8Br_4]^{2+}$	0.060	NHC	S24
$[Au_{13}(iPr\text{-}Bzim)_6Br_6]^{-}$	0.022	NHC	S25
$[Au_{13}(\mu\text{-}(CH_2)_3\text{-}bis\text{-}Bzim^{Bn})_5Br_2]^{3+}$	0.033	NHC	S25
$[Au_{13}(Bzim^{Py})_9Cl_3]^{2+}$	0.022	NHC	S25
$[Au_{13}(\mu\text{-}(CH_2)_3\text{-}bis\text{-}Bzim^{Bn})_3(tpp)_3Cl_2]^{3+}$	0.095	NHC	S26
$[Au_{13}(\mu\text{-}(M/P\text{-}o\text{-}xylyl)\text{-}bis\text{-}Bzim^{Bn})_5Cl_2]^{3+}$	0.023	NHC	S27

$[Au_{13}(\mu\text{-(m-Ph)-bis-Bzim}^{Me})_5Br_2]^{3+}$	0.138	NHC	S28
$[Au_{13}(\mu\text{-(m-Ph)-bis-Bzim}^{Et})_5Br_2]^{3+}$	0.151	NHC	S28
$[Au_{13}(\mu\text{-(m-Ph)-bis-Bzim}^{3,5\text{-Me2Bn}})_5Br_2]^{3+}$	0.162	NHC	S28
$[Au_{13}(\text{bis-Bzim}^{Bn}\text{-COOH})_5Cl_2]^{3+}$	0.023	NHC	S29
$[Au_{13}(\text{bis-NHC}^{Bn})_5Cl_2]^{3+}$	0.020	NHC	S30
$[PdAu_{12}(\text{Bzim}^{Bn})_9Cl_3]^{+}$	0.020	NHC	S31
$[Au_{25}(PET)_{18}]^{-}$	0.063	thiolate	S32
$[Au_{25}(PhSe)_{18}]^{-}$	0.057	selenolate	S33
$[Au_{25}(FPA)_{18}]^{-}$	0.028	alkynyl	S34
$[CdAu_{24}(PA)_{18}]^{0}$	0.078	alkynyl	S35
$[HgAu_{24}(PA)_{18}]^{0}$	0.092	alkynyl	S35
$[PtAu_{24}(PA)_{18}]^{0}$	0.245	alkynyl	S35
$[PtAu_{24}(PET)_{18}]^{0}$	0.348	thiolate	S36
$[PtAu_{24}(PET)_{18}]^{-}$	0.053	thiolate	S36
$[PtAu_{24}(PET)_{18}]^{2-}$	0.019	thiolate	S36
$[PtCdAu_{23}(PET)_{18}]^{-}$	0.026	thiolate	S37
$[CdAu_{24}(PET)_{18}]^{0}$	0.040	thiolate	S38

*For detailed structures, refer to each literature.

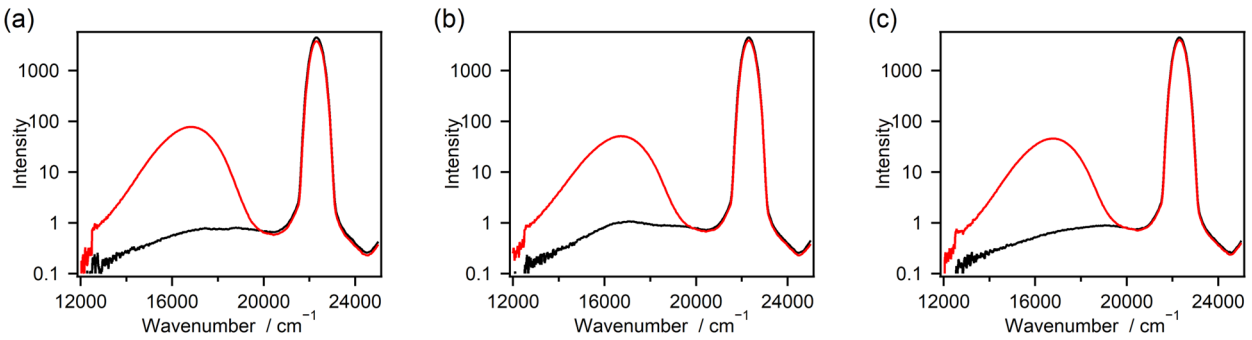

Fig. S5 Photoluminescence spectra of **IrAu$_{12}$-b** excited by 450-nm light in (a) CH_2Cl_2, (b) CH_3CN, and (c) MeOH for the estimation of PLQY by the absolute method. Black and red lines show the observed signal without and with samples, respectively.

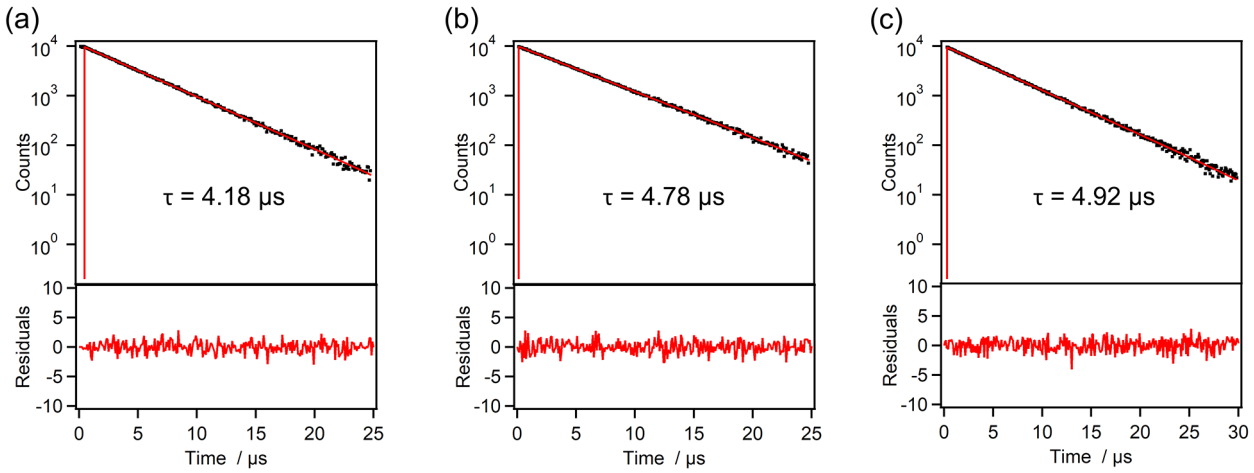

Fig. S6 Photoluminescence lifetime of **IrAu$_{12}$-b** upon 367-nm light irradiation in (a) CH_2Cl_2, (b) CH_3CN, and (c) MeOH.

Table S2 PLQY and Lifetime Values of **IrAu$_{12}$-b** in CH_2Cl_2, CH_3CN, and MeOH

	CH_2Cl_2	CH_3CN	MeOH
PLQY	0.87	0.76	0.77
Lifetime (μs)	4.18	4.78	4.92

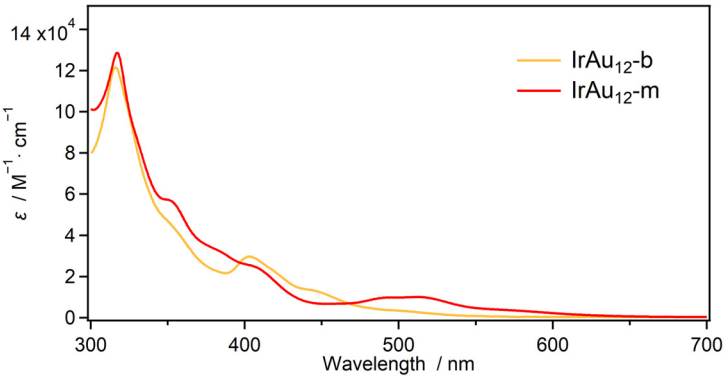

Fig. S7 Molar absorptivity of **IrAu$_{12}$-m** and **IrAu$_{12}$-b**.

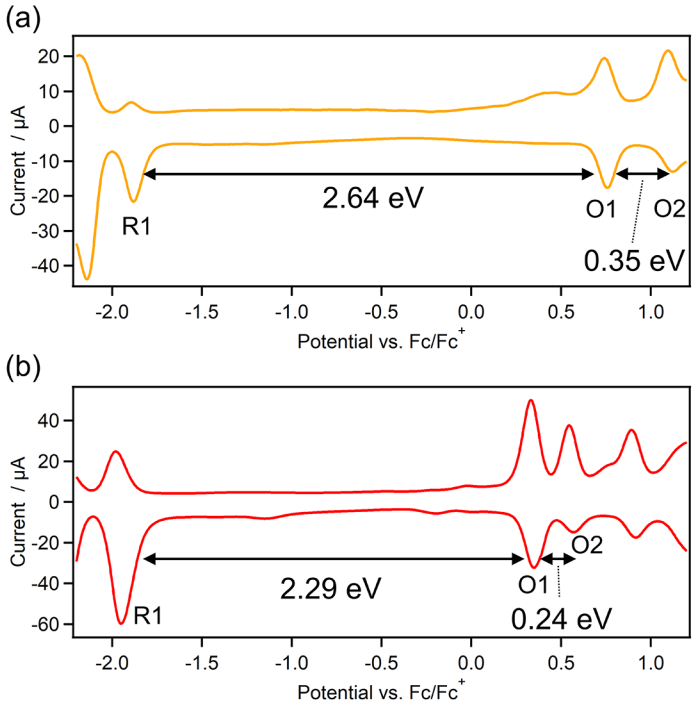

Fig. S8 DPV measurements of (a) **IrAu$_{12}$-b** and (b) **IrAu$_{12}$-m** in CH_2Cl_2 containing 0.1 M $TBAPF_6$ at room temperature.

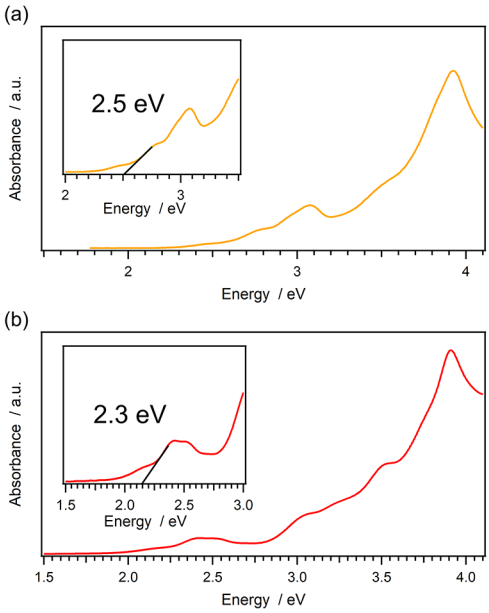

Fig. S9 Optical energy gaps for (a) **IrAu$_{12}$-b** and (b) **IrAu$_{12}$-m** estimated from the absorption spectra.

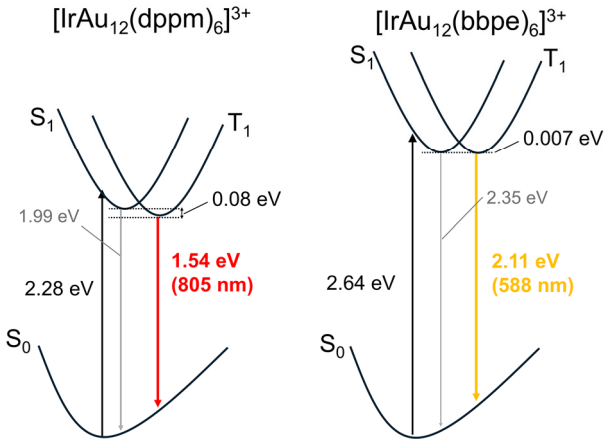

Fig. S10 Energy diagrams for S_0, S_1 and T_1 states of **IrAu$_{12}$-m** and **IrAu$_{12}$-b** estimated by the DFT calculation.

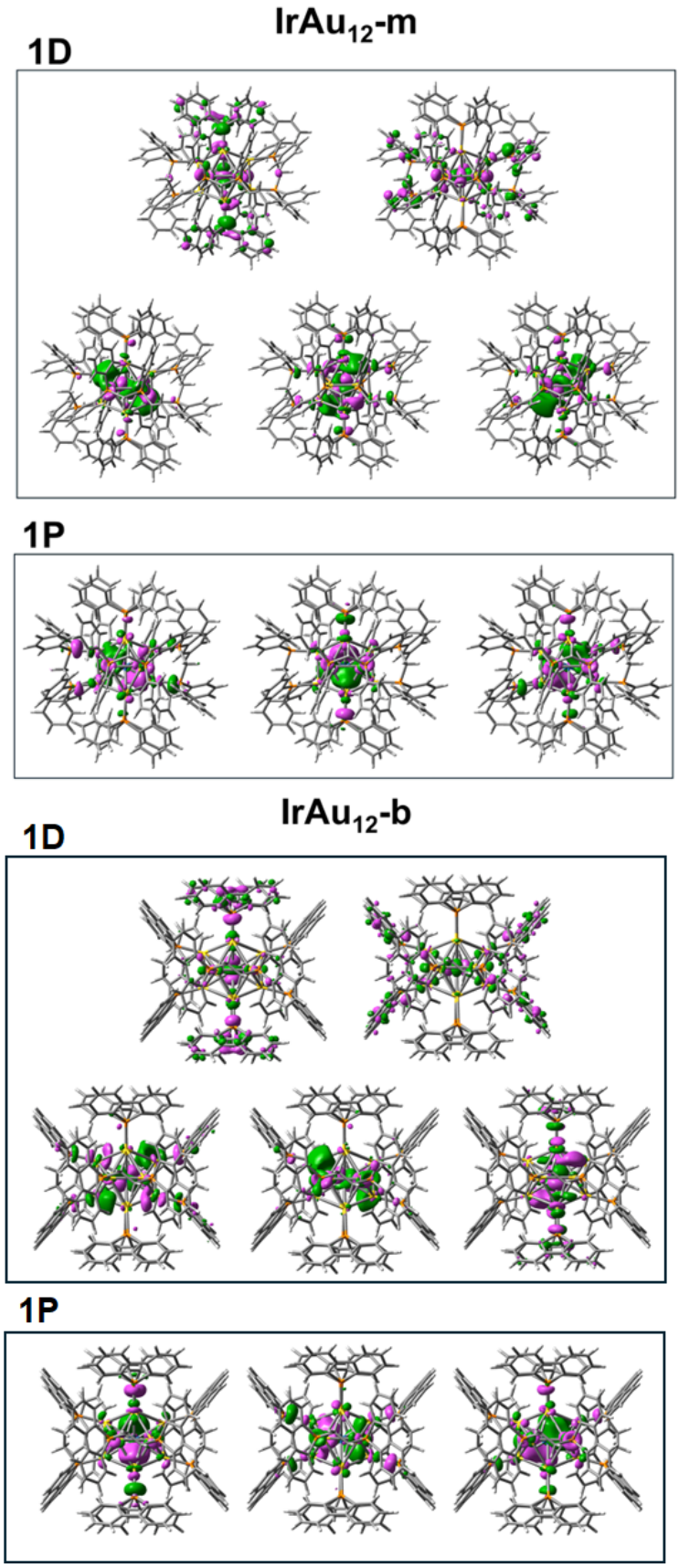

Fig. S11 Kohn-Sham orbitals for **$IrAu_{12}$-m** and **$IrAu_{12}$-b**.

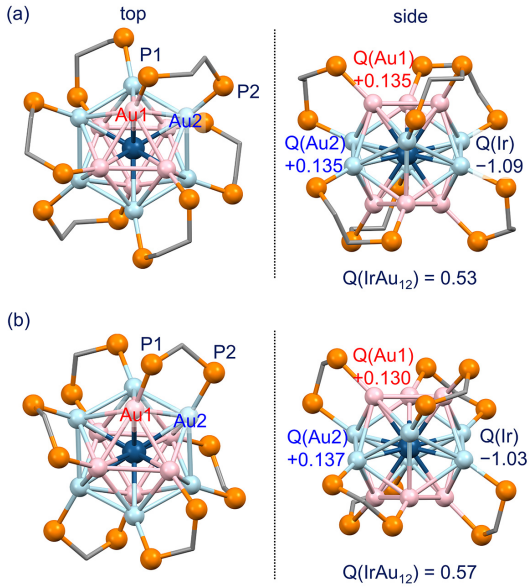

Fig. S12 Natural charges of the Ir@Au12 core of (a) **IrAu12-b**, (b) **IrAu12-m**.

Table S3 Crystallographic Parameters of **$IrAu_{12}$-b**

Empirical formula	$C_{168}H_{144}Au_{12}Cl_{24}F_{12}IrP_{14}$
Formula weight	6231.00
Temperature	100.0(5) K
Wavelength	0.71073 Å
Crystal system	trigonal
Space group	R-3
Unit cell dimensions	a = 18.8392(3) Å α = 90°
	b = 18.8392(3) Å β = 90°
	c = 46.1573(13) Å γ = 120°
Volume	114187.2(6) $Å^3$
Z	3
Density (calculated)	2.188 g/cm^3
Absorption coefficient	10.483 mm^{-1}
F(000)	8709.0
Theta range for data collection	3.06 to 50.74°
Index ranges	-20<=h<=22, -22<=k<=22, -55<=l<=52
Reflections collected	49960
Independent reflections	5794 [R(int) = 0.0270]
Data / restraints / parameters	5795 / 518 / 354
Goodness-of-fit on F^2	1.116
Final R indices [I>2sigma(I)]	R1 = 0.0355, wR2 = 0.1024
R indices (all data)	R1 = 0.0387, wR2 = 0.1047
Largest diff. peak and hole	1.65 and -2.41 $eÅ^{-3}$

Reference

S1. Gaussian 16, Revision C.02, M. J. Frisch, G. W. Trucks, H. B. Schlegel, G. E. Scuseria, M. A. Robb, J. R. Cheeseman, G. Scalmani, V. Barone, G. A. Petersson, H. Nakatsuji, X. Li, M. Caricato, A. V. Marenich, J. Bloino, B. G. Janesko, R. Gomperts, B. Mennucci, H. P. Hratchian, J. V. Ortiz, A. F. Izmaylov, J. L. Sonnenberg, D. Williams-Young, F. Ding, F. Lipparini, F. Egidi, J. Goings, B. Peng, A. Petrone, T. Henderson, D. Ranasinghe, V. G. Zakrzewski, J. Gao, N. Rega, G. Zheng, W. Liang, M. Hada, M. Ehara, K. Toyota, R. Fukuda, J. Hasegawa, M. Ishida, T. Nakajima, Y. Honda, O. Kitao, H. Nakai, T. Vreven, K. Throssell, J. A. Montgomery, Jr., J. E. Peralta, F. Ogliaro, M. J. Bearpark, J. J. Heyd, E. N. Brothers, K. N. Kudin, V. N. Staroverov, T. A. Keith, R. Kobayashi, J. Normand, K. Raghavachari, A. P. Rendell, J. C. Burant, S. S. Iyengar, J. Tomasi, M. Cossi, J. M. Millam, M. Klene, C. Adamo, R. Cammi, J. W. Ochterski, R. L. Martin, K. Morokuma, O. Farkas, J. B. Foresman, and D. J. Fox, Gaussian, Inc., Wallingford CT, 2016.

S2. E. D. Glendening, J, K. Badenhoop, A. E. Reed, J. E. Carpenter, J. A. Bohmann, C. M. Morales, P. Karafiloglou, C. R. Landis, and F. Weinhold, Theoretical Chemistry Institute, University of Wisconsin, Madison (2018).

S3. G. M. Sheldrick, *Acta Cryst. C,* 2015, **71**, 3–8.

S4. P. van der Sluis and A. L. Spek, *Acta Cryst. A,* 1990, **46**, 194–201.

S5. A. L. Spek, *J. Appl. Cryst.* 2003, **36**, 7–13.

S6. S. Takano, H. Hirai, T. Nakashima, T. Iwasa, T. Taketsugu and T. Tsukuda, *J. Am. Chem. Soc.*, 2021, **143**, 10560–10564.

S7. S.-S. Zhang, L. Feng, R. D. Senanayake, C. M. Aikens, X.-P. Wang, Q.-Q. Zhao, C.-H. Tung and D. Sun, *Chem. Sci.*, 2018, **9**, 1251−1258.

S8. Y. Shichibu and K. Konishi, *Small*, 2010, **6**, 1216–1220.

S9. H. Hirai, S. Takano, T. Nakashima, T. Iwasa, T. Taketsugu and T. Tsukuda, *Angew. Chem. Int. Ed.*, 2022, **61**, e202207290.

S10. H. Hirai, S. Takano, T. Nakamura and T. Tsukuda, *Inorg. Chem.*, 2020, **59**, 17889−17895.

S11. H. Hirai, S. Takano, S. Masuda and T. Tsukuda, *ChemElectroChem*, 2024, **11**, e202300669.

S12. M. Sugiuchi, Y. Shichibu, T. Nakanishi, Y. Hasegawa and K. Konishi, *Chem. Commun.*, 2015, **51**, 13519–13522.

S13. Y. Fukumoto, T. Omoda, H. Hirai, S. Takano, K. Harano and T. Tsukuda, *Angew. Chem., Int. Ed.*, 2024, **63**, e202402025.

S14. N. Kito, S. Takano, S. Masuda, K. Harano and T. Tsukuda, *Bull. Chem. Soc. Jpn.*, 2023, **96**, 1045–1051.

S15. Y. Yang, Q. Zhang, Z.-J. Guan, Z.-A. Nan, J.-Q. Wang, T. Jia and W.-W. Zhan, *Inorg. Chem.*, 2019, **58**, 3670–3675.

S16. H. Hirai, T. Nakashima, S. Takano, Y. Shichibu, K. Konishi, T. Kawai and T. Tsukuda, *J. Mater. Chem. C*, 2023, **11**, 3095–3100.

S17. J. Liu, J.-C. Liu, H.-L. Wang, P.-Y. Liao, J.-H. Jia and M.-L. Tong, *Inorg. Chem. Front.*, 2024, **11**, 2553–2561.

S18. Y. Tan, G. Sun, T. Jiang, D. Liu, Q. Li, S. Yang, J. Chai, S. Gao, H. Yu and M. Zhu, *Angew. Chem. Int. Ed.*, 2024, **63**, e202317471.

S19. Y. Zhang, W. Zhang, T.-S. Zhang, C. Ge, Y. Tao, W. Fei, W. Fan, M. Zhou, M.-B. Li, *J. Am. Chem. Soc.*, 2024, **146**, 9631–9639.

S20. J.-H. Yu, Z.-R. Yuan, J. Xu, J.-G. Wang, M. Azam, T.-D. Li, Y.-Z. Li and D. Sun, *Chem. Sci.*, 2023, **14**, 6564–6571.

S21. Y. Shichibu, F. Zhang, Y. Chen, M. Konishi, S. Tanaka, H. Imoto, K. Naka and K. Konishi, *J. Chem. Phys.*, 2021, **155**, 054301.

S22. Y.-Z. Li, R. Ganguly, K. Y. Hong, Y. Li, M. E. Tessensohn, R. Webster and W. K. Leong, *Chem. Sci.*, 2018, **9**, 8723–8730.

S23. M. R. Narouz, S. Takano, P. A. Lummis, T. I. Levchenko, A. Nazemi, S. Kaappa, S. Malola, G. Yousefalizadeh, L. A. Calhoun,

K. G. Stamplecoskie, H. Häkkinen, T. Tsukuda and C. M. Crudden, *J. Am. Chem. Soc.*, 2019, **aa**, 14997–15002.

S24. P. Luo, X.-J. Zhai, S. Bai, Y.-B. Si, X.-Y. Dong, Y.-F. Han and S.-Q. Zang, *Angew. Chem. Int. Ed.*, 2023, **62**, e202219017.

S25. H. Shen, S. Xiang, Z. Xu, C. Liu, X. Li, C. Sun, S. Lin, B. K. Teo and N. Zheng, *Nano Res.*, 2020, **13**, 1908–1911.

S26. M. Bevilacqua, M. Roverso, S. Bogialli, C. Graiff and A. Biffis, *Inorg. Chem.*, 2023, **62**, 1383–1393.

S27. H. Yi, K. M. Osten, T. I. Levchenko, A. J. Veinot, Y. Aramaki, T. Ooi, M. Nambo and C. M. Crudden, *Chem. Sci.*, 2021, **12**, 10436–10440.

S28. P. Luo, S. Bai, X. Wang, J. Zhao, Z. N. Yan, Y. F. Han, S. Q. Zang and T. C. Mak, *Adv. Opt. Mater.*, 2021, **9**, 2001936.

S29. X. Yuan, Z. Ye, S. Malola, O. Shekhah, H. Jiang, X. Hu, J.-X. Wang, H. Wang, A. Shkurenko, J. Jia, V. Guillerm, O. F. Mohammed, X. Chen, N. Zheng, H. Häkkinen and M. Eddaoudi, *Chem. Sci.*, 2024, **15**, 16112–16117.

S30. M. Bevilacqua, M. Roverso, S. Bogialli, C. Graiff and A. Biffis, *Eur. J. Inorg. Chem.*, 2024, **27**, e20240035.

S31. H. Shen, Q. Wu, M. S. A. Hazer, X. Tang, Y.-Z. Han, R. Qin, C. Ma, S. Malola, B. K. Teo, H. Häkkinen and N. Zheng, *Chem*, **8**, 2380–2392

S32. (a) M. W. Heaven, A. Dass, P. S. White, K. M. Holt and R. W. Murray, *J. Am. Chem. Soc.*, 2008, **130**, 3754–3755. (b) M. Zhu, C. M. Aikens, F. J. Hollander, G. C. Schatz and R. Jin, *J. Am. Chem. Soc.*, 2008, **130**, 5883–5885.

S33. Y. Song, J. Zhong, S. Yang, S. Wang, T. Cao, J. Zhang, P. Li, D. Hu, Y. Pei and M. Zhu, *Nanoscale*, 2014, **6**, 13977–13985.

S34. J.-J. Li, Z.-J. Guan, Z. Lei, F. Hu and Q.-M. Wang, *Angew. Chem., Int. Ed.*, 2019, **58**, 1083–1087.

S35. W. Fei, S. Antonello, T. Dainese, A. Dolmella, M. Lahtinen, K. Rissanen, A. Venzo and F. Maran, *J. Am. Chem. Soc.*, 2019, **141**, 16033–16045.

S36. M. Suyama, S. Takano, T. Nakamura and T. Tsukuda, *J. Am. Chem. Soc.*, 2019, **141**, 14048–14051.

S37. M. Suyama, S. Takano and T. Tsukuda, *J. Phys. Chem. C*, 2020, **124**, 23923–23929.

S38. W. Fei, S. Antonello, T. Dainese, A. Dolmella, M. Lahtinen, K. Rissanen, A. Venzo, F. Maran, *J. Am. Chem. Soc.*, 2019, **141**, 16033–16045.